Rare Metal Materials and Engineering
Volume 48, Issue 8, August 2019
Available online at www.rmme.ac.cn

Science Press

Cite this article as: Rare Metal Materials and Engineering, 2019, 48(8): 2400-2405.

ARTICLE

Schmid Factor Maps for Predicting Slip and Twinning Behaviors in Zirconium

Xin Chao, Sun Qiaoyan, Xiao Lin, Sun Jun

State Key Laboratory for Mechanical Behavior of Materials, Xi'an Jiaotong University, Xi'an 710049, China

Abstract: A series of Schmid factor (SF) maps for different slip and twinning modes in zirconium were calculated and illustrated as a function of the tensile angle between the applied stress and the *c*-axis together with the projective angle on the basal plane. The results show that the deformation modes include three groups of slip systems, i.e. basal slip, prismatic slip, pyramidal <*a*> and <*c*+*a*> slip, and four groups of twinning systems, i.e. $\{10\bar{1}2\}$, $\{11\bar{2}1\}$, $\{11\bar{2}2\}$ and $\{10\bar{1}1\}$. The "soft" and "hard" orientation zones of individual plastic deformation modes were determined. A variant selection criterion for slip and twinning of zirconium was proposed. The plastic deformation mechanism was interpreted based on the Schmid factor maps in combination with the experimental data of the critical resolved shear stress (CRSS) under different deformation modes. The predicted plastic deformation mechanism is consistent with the experimental results.

Key words: Schmid law; slip; twinning; variant selection; anisotropy; zirconium

Zirconium and its alloys owning hexagonal closed packed (HCP) crystal structure display excellent ductility during deformation at room temperature even though they have less than five independent plastic deformation modes to fulfill von Mises criterion [1]. The two most common slip systems, prismatic and basal slips, offer only four independent modes. Four independent modes are also provided by the pyramidal slip systems with ***a*** Burgers vector, which are crystallographically equivalent to the combined four independent modes by cross slip between basal and prismatic slip systems[2]. Furthermore, the distribution of these slip systems is asymmetry in the space, and the critical resolved shear stress (CRSS) on different slip planes is significantly different. As a result, anisotropic deformation behavior appears in zirconium and its alloys[3,4]. Up to date, the plastic deformation behavior of zirconium has been the subject of many investigations[5-10]. It is well established that <*a*> slip on $\{10\bar{1}0\}$ prism plane is the most active deformation mode in zirconium with an axial ratio, *c*/*a*, of 1.593 [11]. Other possible slip systems include $\{10\bar{1}1\}$ and $\{11\bar{2}1\}$ pyramidal slip and $\{0001\}$ basal slip. The critical resolved shear stress (CRSS) of pyramidal and basal slips is higher than that of the prismatic slip. As one of primary plastic deformation modes, twinning plays an important role in maintaining the homogeneous plastic deformation in zirconium. Four types of twins have been reported, i.e. $\{10\bar{1}2\}$, $\{11\bar{2}1\}$, $\{11\bar{2}2\}$ and $\{10\bar{1}1\}$ twins.

The Schmid factor (SF) and the CRSS are two vital parameters for determining the activity of different deformation mechanisms under the applied stress. The Schmid factor indicates the hard/soft degree of different deformation modes under certain applied stress orientation. The CRSS is a critical parameter of material for activating certain deformation mode. The Schmid factor distribution in combination with the CRSS can be used to predict the plastic deformation behavior of material[12-15]. The Schmid criterion is expressed as $\sigma_{ys} = \tau_{CRSS}/m$, where τ_{CRSS} is the CRSS for one certain deformation mode, and m is the Schmid factor. The τ_{CRSS} is a parameter of material dependent on deformation temperature, strain rate, impurity etc[16-18].

Received date: August 18, 2018
Foundation item: National Natural Science Foundation of China (51471129, 51671158, 51621063); "973" Program of China (2014CB644003); "111" Project of China (B06025)
Corresponding author: Sun Qiaoyan, Ph. D., Professor, State Key Laboratory for Mechanical Behavior of Materials, Xi'an Jiaotong University, Xi'an 710049, P. R. China, Tel: 0086-29-82665125, E-mail: qysun@mail.xjtu.edu.com

The SF value is usually calculated and expressed in stereographic triangles with orientation index[19,20]. However, Nan et al[21] systematically calculated SFs as a function of angle between the *c*-axis and the loading direction and the selected three projective locations on the basal plane, (0°, 15°, and 30°), relative to the loading direction for different deformation mechanisms in magnesium. An angle between the a_1-axis and the projected location of the loading direction on the basal plane was introduced in this work to establish a comprehensive SF distribution map. In combination with the experimental data of the CRSS, these SF maps can be used to predict the plastic deformation mechanism, the yielding anisotropy, and variant selection effect in zirconium.

1 Experiment

Typical slip modes in zirconium and zircaloy include <*a*> slip on basal $\{0001\}$, prismatic $\{10\bar{1}0\}$ and pyramidal $\{10\bar{1}1\}$ planes, and <*c*+*a*> slip on pyramidal $\{10\bar{1}1\}$ and $\{11\bar{2}1\}$ planes. The twinning modes consist of two types of tensile twinning $\{10\bar{1}2\}<\bar{1}011>$ and $\{11\bar{2}1\}<\bar{1}\bar{1}26>$, and two types of compression twinning $\{11\bar{2}2\}<11\bar{2}3>$ and $\{10\bar{1}1\}<10\bar{1}\bar{2}>$. For a specific deformation mode (slip or twinning), (*hkil*) [*uvtw*], the slip or twinning plane normal with 3-index is given by:

$$[h_1k_1l_1]=\left[2h+k,h+2k,\frac{3l}{2}(\frac{a}{c})^2\right] \quad (1)$$

where *a* and *c* are the lattice parameters, equal to 0.3232 and 0.5147 nm for zirconium with a *c*/*a* axial ratio of 1.593, respectively. The slip or twinning direction with 3-index is expressed as:

$$[u_1v_1w_1]=[u-t,v-t,w] \quad (2)$$

The loading direction can be expressed with two angles of α and θ, as shown in Fig.1. θ is an angle between the *c*-axis and the loading direction. α represents an angle between the a_1-axis and the projected location of the loading direction on the basal plane. The clockwise direction is set as positive. The loading direction can be expressed by 3-index as follows:

$\theta=0°$: $[u_2v_2w_2]=[001]$

$\theta\in(0°,90°)$:

$$\left[\cos\alpha+\cos(60°+\alpha),\cos(60°+\alpha)-\cos(60°-\alpha),\frac{3}{2\tan\theta}(\frac{a}{c})\right]$$

$\theta=90°$:

$$[\cos\alpha+\cos(60°+\alpha),\cos(60°+\alpha)-\cos(60°-\alpha),0] \quad (3)$$

The cosine functions $\cos\phi$ and $\cos\lambda$ can then be calculated by:

$$\cos\phi(\lambda)=\frac{\left[u_1u_2+v_1v_2-\frac{1}{2}(u_1v_2+u_2v_1)+(\frac{c}{a})^2w_1w_2\right]}{\left[\left(u_1^2+v_1^2-u_1v_1+(\frac{c}{a})^2w_1^2\right)\left(u_2^2+v_2^2-u_2v_2+(\frac{c}{a})^2w_2^2\right)\right]^{\frac{1}{2}}} \quad (4)$$

The calculation of Schmid factor is carried out in MATLAB software. It is worth noting that twinning is a polar mechanism, which only allows simple shear in one direction, different from slip. Therefore, the absolute value of *m* is used for dislocation slip, which allows dislocation to move forward and backward.

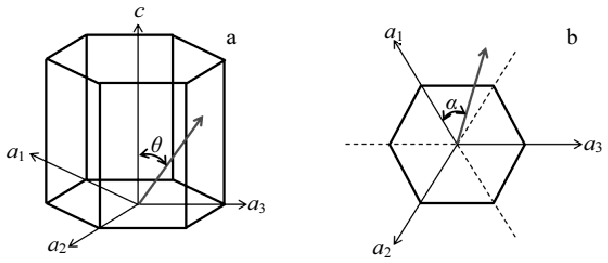

Fig.1 Schematic diagram of loading axis: (a) relation of loading axis and *c*-axis and (b) projected location of the relative loading direction on the basal plane

2 Result and Discussion

2.1 Schmid factor maps of individual slip and twinning systems

Figs.2a~2e show the SF maps as function of two directions of α and θ for each individual slip system, which includes $(0001)[1\bar{2}10]$ basal slip, $(10\bar{1}0)[1\bar{2}10]$ prismatic slip, $(10\bar{1}1)[1\bar{2}10]$ first-order pyramidal <*a*> slip, $(01\bar{1}1)[1\bar{2}13]$ first-order pyramidal <*c*+*a*> slip and $(11\bar{2}1)[1\bar{2}13]$ second-order pyramidal <*c*+*a*> slip. Elliptical distribution for (0001) basal <*a*> slip is displayed. The maximum SF, *m*=0.5, is located at the center of each ellipse where both the [0001] and $[1\bar{2}10]$ directions have the same θ angle of 45° to the applied stress direction, as indicated by black solid dots in Fig.2a. With regards to $(10\bar{1}0)$ prismatic <*a*> slip, semi-elliptical distribution is displayed. The maximum SF, *m*=0.5, is located at the center of each ellipse, where the θ is equal to 90°, as indicated by black solid dots in Fig.2b. Asymmetric elliptical distribution of the SF for $(01\bar{1}1)$ pyramidal <*a*> slips is displayed, as shown in Fig.2c. For $[1\bar{2}10]$ slip on (0001) basal planes, $(10\bar{1}0)$ prismatic and $(10\bar{1}1)$ pyramidal planes, the SF shows symmetric distribution, and the common symmetry axis is α=150° and 330°, where the stress direction is normal to the slip direction $[1\bar{2}10]$. In contrast, no symmetry is visible for pyramidal <*c*+*a*> slip (Fig.2d and 2e). For $[1\bar{2}13]$ slip on $(01\bar{1}1)$ first-order pyramidal plane and $(11\bar{2}1)$ second-order pyramidal plane, their SF distributions are very similar because of the same slip direction $[1\bar{2}13]$, even though the high SF zones are located at different areas.

Fig.3a~3d show the SF distribution as a function of α and θ for each individual twin system. The twins include $(0\bar{1}12)[01\bar{1}1]$ and $(\bar{1}2\bar{1}1)[1\bar{2}16]$ tensile twinning, $(1\bar{2}12)[1\bar{2}1\bar{3}]$ and $(0\bar{1}11)[0\bar{1}1\bar{2}]$ compressive twinning. Significant differences are displayed between slip and twinning systems. The negative SF value appears in the SF maps of twinning system. It indicates that the twin cannot be activated under these orientations. Moreover, the SF maps of each slip system

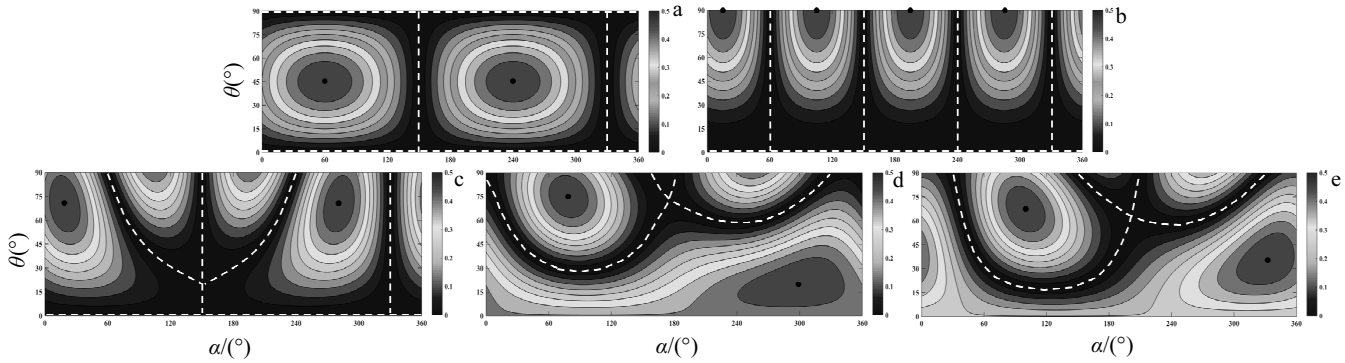

Fig.2 Schmid factor distribution map for each individual slip system: (a) $(0001)[1\bar{2}10]$, (b) $(10\bar{1}0)[1\bar{2}10]$, (c) $(10\bar{1}1)[1\bar{2}10]$, (d) $(01\bar{1}1)[1\bar{2}13]$, and (e) $(11\bar{2}1)[1\bar{2}13]$

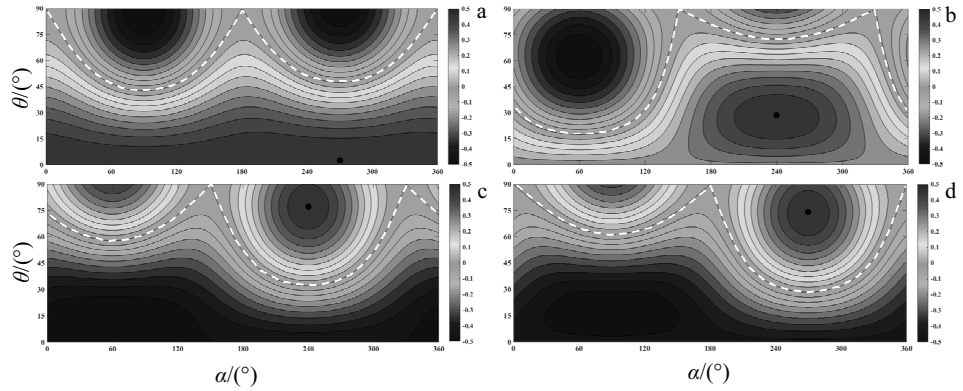

Fig.3 Schmid factor distribution maps for tensile twinning $(0\bar{1}12)[01\bar{1}1]$ (a) and $(\bar{1}2\bar{1}1)[1\bar{2}16]$ (b), and compression twinning $(1\bar{2}12)[1\bar{2}1\bar{3}]$ (c) and $(0\bar{1}11)[0\bar{1}1\bar{2}]$ (d)

have at least two high SF zones, while only one high SF zone is observed for twinning system.

High SF zone of $m\geq0.450$ is defined as "soft" orientation zone in terms of the resolved shear stress, which is higher in "soft" zone than in the rest zones under the same applied stress, as marked with the red color in Fig.2a~2e and Fig.3a~3d. The area fraction of "soft" orientation zone is quantitatively calculated, as listed in Table 1.

It is revealed that the $(0\bar{1}12)[01\bar{1}1]$ tensile twin has the largest area fraction of "soft" orientation zone, which is concentrated within the area of $\theta<20°$. While the area fractions of "soft" zone for two compression twins $\{11\bar{2}2\}<11\bar{2}3>$ and $\{10\bar{1}1\}<10\bar{1}2>$ are the smallest, which implies that they are the hardest to be activated under tensile stress. Other slips and twins have similar area fraction of about 5% "soft" zone except the $(01\bar{1}1)[1\bar{2}13]$ slip is 9.46%. In comparison, the low SF area ($m\leq0.05$) is defined as the "hard" orientation, as marked with dark blue zones in Fig.2a~2e and Fig.3a~3d. The minimum values ($m=0$) are marked with white dashed lines. It means that these deformation modes cannot be activated in these orientations, as shown in Fig.2 and Fig.3.

Table 1 Area fraction of "soft" orientation zone for individual slip and twinning systems

Deformation mode		Area fraction/%
Slip	$(0001)[1\bar{2}10]$	6.53
	$(10\bar{1}0)[1\bar{2}10]$	4.64
	$(10\bar{1}1)[1\bar{2}10]$	4.95
	$(01\bar{1}1)[1\bar{2}13]$	9.46
	$(11\bar{2}1)[1\bar{2}13]$	6.55
Twinning	$(0\bar{1}12)[01\bar{1}1]$	16.9
	$(\bar{1}2\bar{1}1)[1\bar{2}16]$	5.00
	$(1\bar{2}12)[1\bar{2}1\bar{3}]$	2.37
	$(0\bar{1}11)[0\bar{1}1\bar{2}]$	2.41

2.2 Variant selection for individual slip and twinning systems

It is well-known that each slip and twin systems have several variants (geometrical equivalent deformation mode). We integrate the SFs maps of all variants into one formula according to the criterion as follows:

$$SF_{(\alpha,\theta)} = \max(SF^1_{(\alpha,\theta)}, SF^2_{(\alpha,\theta)}, \cdots, SF^n_{(\alpha,\theta)}) \quad (5)$$

where n is the number of variant, as shown in Fig.4 and Fig.5. The orientation relation of "soft" orientation zone (high SF)

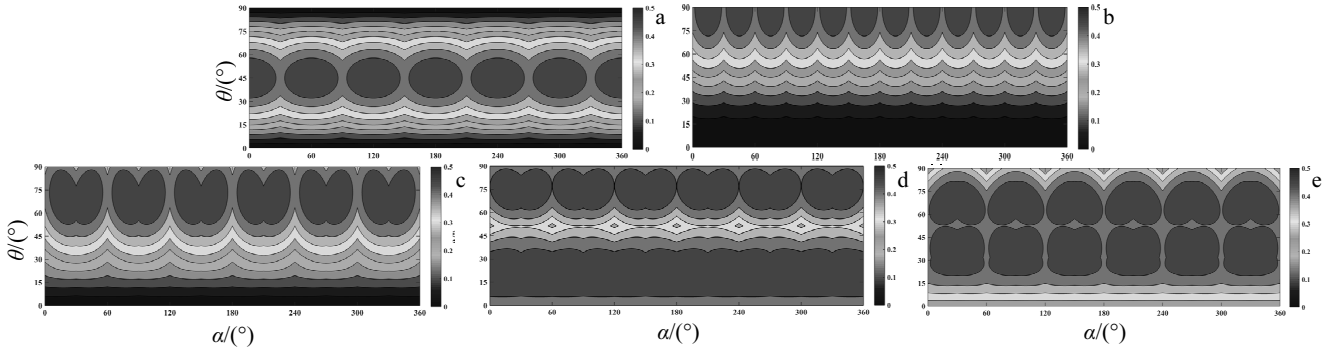

Fig.4 Schmid factor distribution map for each individual slip system: (a) $\{0001\}\langle 11\bar{2}0\rangle$, (b) $\{10\bar{1}0\}\langle 11\bar{2}0\rangle$, (c) $\{10\bar{1}1\}\langle 11\bar{2}0\rangle$, (d) $\{10\bar{1}1\}\langle 11\bar{2}3\rangle$, and (e) $\{11\bar{2}1\}\langle 11\bar{2}3\rangle$

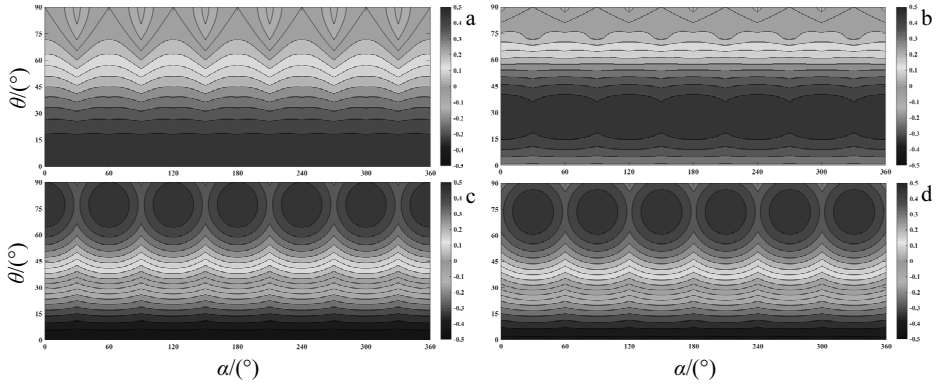

Fig.5 Schmid factor distribution map for each individual twinning system: (a) $\{10\bar{1}2\}\langle\bar{1}011\rangle$, (b) $\{11\bar{2}1\}\langle\bar{1}\bar{1}26\rangle$, (c) $\{11\bar{2}2\}\langle 11\bar{2}\bar{3}\rangle$, and (d) $\{10\bar{1}1\}\langle 10\bar{1}2\rangle$

between different variants can be distinguished. Different deformation modes will be activated with the variation of θ, while the different slip and twinning system variants will be displayed with the variation of α. When the applied stress is located at the overlap area of two or more "soft" zones of variants, the double or multiple slip or twinning will be activated at the same time. The area fraction of "soft" orientation zone is also quantitatively calculated, as listed in Table 2. It is revealed that the <*c*+*a*> slip on pyramidal $\{10\bar{1}1\}$ and $\{11\bar{2}1\}$ planes has the largest area fraction of "soft" orientation zone. While the $\{10\bar{1}2\}\langle\bar{1}011\rangle$ tensile twin has the largest overlap area between its variants. This means that the variant selection for slip and twin can be interpreted based on these SF maps of zirconium.

Table 2 Area fraction of "soft" orientation zone for individual slip and twinning systems including geometrical equivalent variants

Deformation mode		Area fraction/%
Slip	$\{0001\}\langle 11\bar{2}0\rangle$	19.59
	$\{10\bar{1}0\}\langle 11\bar{2}0\rangle$	13.92
	$\{10\bar{1}1\}\langle 11\bar{2}0\rangle$	14.8
	$\{10\bar{1}1\}\langle 11\bar{2}3\rangle$	58.2
	$\{11\bar{2}1\}\langle 11\bar{2}3\rangle$	54.2
Twinning	$\{10\bar{1}2\}\langle\bar{1}011\rangle$	20.6
	$\{11\bar{2}1\}\langle\bar{1}\bar{1}26\rangle$	26.1
	$\{11\bar{2}2\}\langle 11\bar{2}\bar{3}\rangle$	14.2
	$\{10\bar{1}1\}\langle 10\bar{1}2\rangle$	14.5

2.3 Interpretation of deformation mechanisms in zirconium under the applied stress

The activity and selection of deformation modes in the zirconium subjected to applied stress are dependent on the SF and τ_{CRSS} according to the Schmid law. Each deformation mode has a "soft" zone with high SF value, where the slip or twin is easy to be activated. According to the calculated SF maps, high SF zone or "soft" zone is summarized in Table 3. Most "soft" deformation zones overlap each other, indicating that they have the high SF values under the same stress direction. The deformation mode with the lower τ_{CRSS} will be activated prior to others if they have the same SF. For instance, two pyramidal <*c*+*a*> slips of $\{11\bar{2}1\}\langle 11\bar{2}3\rangle$ and $\{10\bar{1}1\}\langle 11\bar{2}3\rangle$, pyramidal <*a*> and prismatic <*a*> slip have similar SF value when the direction is nearly perpendicular to the *c*-axis, while the prismatic <*a*> slip is firstly activated prior to pyramidal slip because of its lowest τ_{CRSS}. Alternatively,

Table 3 High SF zone of different deformation modes

Deformation mode		High SF zone, θ
Slip	$\{0001\}<11\bar{2}0>$	(32°, 58°)
	$\{10\bar{1}0\}<11\bar{2}0>$	(71.6°, 90°)
	$\{10\bar{1}1\}<11\bar{2}0>$	(52.5°, 88.1°)
	$\{10\bar{1}1\}<11\bar{2}3>$	(6.4°, 36.7°)
		(61.6°, 88.2°)
	$\{11\bar{2}1\}<11\bar{2}3>$	(20°, 52.2°)
		(53.1°, 81.6°)
Twinning	$\{10\bar{1}2\}<\bar{1}011>$	(0°, 18.7°)
	$\{11\bar{2}1\}<\bar{1}\bar{1}26>$	(14.6°, 40.5°)
	$\{11\bar{2}2\}<11\bar{2}\bar{3}>$	(64.2°, 90°)
	$\{10\bar{1}1\}<10\bar{1}\bar{2}>$	(60.6°, 86.5°)

suitable orientation can be chosen from the SF maps. The Schmid factor for one system should be sufficiently high compared to others so that the slip system can be activated on the desired plane.

For different deformation modes, the yield stress can be expressed under the stress direction (α, θ) according to the Schmid law. While the yield stress of material is calculated by the following equation:

$$\sigma_{(\alpha,\theta)} = \min(\sigma^1_{(\alpha,\theta)},\ \sigma^2_{(\alpha,\theta)},\ \cdots,\ \sigma^n_{(\alpha,\theta)}) \quad (6)$$

The deformation mode with the lowest σ will be the preferential deformation mode. On the one hand, the m (SF) is a stress orientation-dependent parameter for different deformation modes. On the other hand, the τ_{CRSS} is a constant of material independent of the stress direction. It is affected by the temperature, strain rate, impurity etc.[22,23]. Therefore, the plastic deformation behaviors and the variant selection for individual slip and twinning systems in zirconium can be predicted based on the combination of the SF map and the experimental τ_{CRSS} values. The variation of τ_{CRSS} for different deformation modes with temperature in pure Zr is shown in Fig.6 according to Ref.[24-27].

Fig.7 shows the variation of deformation mode with the stress direction and the testing temperature. At room temperature, the dominant deformation mode is prismatic <a> slip

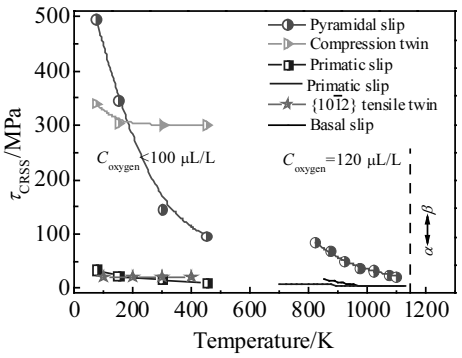

Fig.6 Variation of τ_{CRSS} with temperature for different deformation modes in zirconium with different oxygen contents

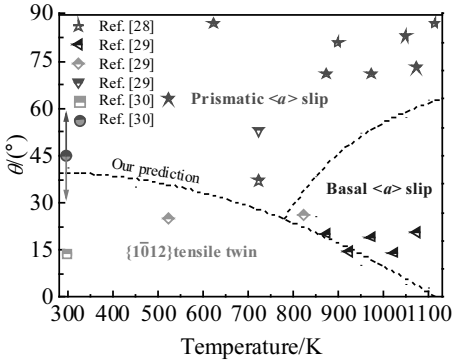

Fig.7 Deformation mode transformation with temperature in zirconium single crystal

and $\{10\bar{1}2\}$ tensile twin. The prismatic <a> slip takes place when θ>45°, while the $\{10\bar{1}2\}$ tensile twin takes place when θ<45°. Moreover, the activity of prismatic <a> slip increases with temperature due to the decrease of the τ_{CRSS}. The τ_{CRSS} of basal slip is similar to that of the prismatic slip when the testing temperature reaches about 800 K. As a result, the basal slip is activated at temperatures over 800 K. The dominant deformation mode has a transition with temperature from prismatic slip+twin to prismatic slip+basal slip at about 800 K. Fig.7 also compares the predicted results with the experimental results in single crystal from different investigators [28-30]. A good agreement is displayed.

It is worth noting that the pyramidal <c+a> slip does not appear in Fig.7, while it has been observed under deformation with certain constraints or at high temperatures [16,29]. It is because the τ_{CRSS} of pyramidal slip is about more than 10 times higher than that of prism <a> slip at different temperatures (Fig.6). The further study is needed in the future.

3 Conclusions

1) The Schmid factor maps in zirconium as a function of the tensile angle between the applied stress and the c-axis together with the projective angle on the basal plane are systematically calculated under different deformation modes. The “soft” and “hard” orientation zones, which indicate the difficulty of plastic deformation under different deformation modes, can be distinguished.

2) The area fraction and location of high SF zone are two important characteristics in SF distribution map. They play key roles in determining deformation mode. The tensile angle between the applied stress and the c-axis, θ, determines the selection of slip and twinning systems, while the projective angle on the basal plane, α, determines the variant selection of individual slip and twinning systems.

3) Based on SF map in combination with the experimental critical resolved shear stress, different deformation mechanisms and their variation selection with temperature are

interpreted. The deformation mode transformation in zirconium can be predicted. The predominant deformation mode has a transformation with temperature from prismatic slip+twin to prismatic slip+basal slip at about 800 K.

References

1 Groves G W, Kelly A A. *Journal of Theoretical Experimental and Applied Physics*[J], 1963, 8(89): 877
2 Yoo M H. *Metall Trans A*[J], 1981,12(3): 409
3 Murty K L, Charit I. *Prog Nucl Energ*[J], 2006, 48(4): 325
4 Ciurchea D. *J Nucl Mater*[J],1985,131(1): 1
5 Erich Tenckhoff. *Deformation Mechanisms, Texture, and Anisotropy in Zirconium and Zircaloy*[M]. Philadelphia: ASTM Special Technical Publication, 1988
6 He W J, Yuan G H, Luan B F *et al*. *Rare Metal Materials and Engineering*[J], 2018, 47(1): 82
7 Singh J, Mahesh S, Roy S *et al*. *Acta Mater*[J], 2017, 123: 337
8 Fuloria D, Nageswararao P, Jayaganthan R *et al*. *Mater Chem Phys*[J], 2016, 173: 12
9 Knezevic M, Zecevic M, Beyerlein I J *et al*. *Acta Mater*[J], 2015, 88: 55
10 Goel S, Keskar N, Jayaganthan R *et al*. *Mater Sci Eng A*[J], 2014, 603: 23
11 Fisher E S, Renken C J. *Phys Rev*[J], 1964, 135: 482
12 Sun Q Y, Guo Q, Yao X *et al*. *Scripta Mater*[J], 2011, 65(6): 473
13 Rawat S, Mitra N. *Comput Mater Sci*[J], 2018, 141: 302
14 Hagihara K, Nakano T, Maki H *et al*. *Sci Rep*[J], 2016, 6: 29 779
15 Chapuis A, Driver J H. *Acta Mater*[J], 2011, 59(5): 1986
16 Gong J C, Britton T B, Cuddihy M A *et al*. *Acta Mater*[J], 2015, 96: 249
17 Rapperport E J. *Acta Metall*[J], 1959, 7(4): 254
18 Wang L, Zheng Z, Phukan H *et al*. *Acta Mater*[J], 2017, 132: 598
19 Wang J T, Stanford N. *Mater Sci Eng A*[J], 2017, 696: 42
20 Wu B L, Wan G, Du X H *et al*. *Mater Sci Eng A*[J], 2013, 573: 205
21 Nan X L, Wang H Y, Zhang L *et al*. *Scripta Mater*[J], 2012, 67(5): 443
22 Long F, Xu F, Daymond M R. *Metall Mater Trans A*[J], 2013, 44(9): 4183
23 Tahreen N, Zhang D F, Pan F S *et al*. *J Alloy Compd*[J], 2016, 688: 270
24 Soo P, Higgins G T. *Acta Metall*[J], 1968, 16(2): 177.
25 Goodrich D G. *Dissertation for Doctorate*[D]. Oregon: Oregon State University, 1970
26 Akhtar A. *J Nucl Mater*[J], 1973, 47(1): 79
27 Beyerlein I J, Tomé C N. *Int J Plast*[J], 2008, 24(5): 867
28 Akhtar A. *Metall Trans A*[J], 1975, 6(6): 1217
29 Akhtar A. *Acta Metall*[J], 1973, 21(2): 1
30 Akhtar A, Teghtsoonian A. *Acta Metall*[J], 1971, 19(7): 655

施密特因子分布图预测锆的变形行为

辛 超，孙巧艳，肖 林，孙 军

(西安交通大学 金属材料强度国家重点实验室，陕西 西安 710049)

摘 要：由拉伸应力方向与 *c* 轴夹角及拉伸应力方向在基面投影与基面 *a* 轴夹角为自变量绘制了锆及锆合金中不同变形方式的施密特因子分布图并做了分析和研究。变形方式包括基面滑移，柱面滑移和锥面滑移的<*a*>和<*c*+*a*>滑移系和{$10\bar{1}2$}，{$11\bar{2}1$}，{$11\bar{2}2$}和{$10\bar{1}1$}4 组孪晶系。每个独立变形方式下的软取向和硬取向被确定。施密特因子分布图结合实验中每种变形方式的临界剪切应力可以有效预测每种变形方式的相对活性并能够很好地吻合现有的实验结果。

关键词：施密特定律；滑移；孪晶；变体选择；各向异性；锆

作者简介：辛 超，男，1988 年生，博士，西安交通大学金属材料强度国家重点实验室，陕西 西安 710049，电话：029-82665125，E-mail: xinchao2013@stu.xjtu.edu.cn